Characterization of nucleation during laboratory earthquakes

S. Latour,[1] A. Schubnel,[1] S. Nielsen,[2,3] R. Madariaga,[1] and S.Vinciguerra[4,5]

Received 31 July 2013; revised 17 September 2013; accepted 19 September 2013; published 4 October 2013.

[1] We observe the nucleation phase of in-plane ruptures in the laboratory. We show that the nucleation is composed of two distinct phases, a quasi-static and an acceleration stage, followed by dynamic propagation. We propose an empirical model which describes the rupture length evolution: The quasi-static phase is described by an exponential growth while the acceleration phase is described by an inverse power law of time. The transition from quasi-static to accelerating rupture is related to the critical nucleation length, which scales inversely with normal stress in accordance with theoretical predictions, and to a critical surfacic power, which may be an intrinsic property of the interface. Finally, we discuss these results in the frame of previous studies and propose a scaling up to natural earthquake dimensions. **Citation:** Latour, S., A. Schubnel, S. Nielsen, R. Madariaga, and S. Vinciguerra (2013), Characterization of nucleation during laboratory earthquakes, *Geophys. Res. Lett.*, *40*, 5064–5069, doi:10.1002/grl.50974.

1. Introduction

[2] Studying the slow nucleation phase that precedes dynamic rupture propagation is of first importance to understand the initiation of earthquake sources. The nucleation phase in mode II was first observed experimentally on Westerly granite [*Dieterich*, 1978; *Okubo and Dieterich*, 1984; *Ohnaka and Shen*, 1999], more recently at an interface between two polycarbonate blocks [*Nielsen et al.*, 2010; *Kaneko and Ampuero*, 2011] and between Sierra White granite [*McLaskey and Kilgore*, 2013]. Continuing early studies of slip instability [e.g., *Ida*, 1972; *Andrews*, 1976], a body of theoretical work has improved our understanding of rupture nucleation in the last two decades [*Campillo and Ionescu*, 1997; *Uenishi and Rice*, 2003; *Rubin and Ampuero*, 2005; *Ampuero and Rubin*, 2008; *Kaneko and Ampuero*, 2011], confirming that a critical nucleation length exists and that it can be related to fault properties. In the late 1990s, the possible signature of a nucleation phase in seismic records of natural earthquakes was discussed [*Iio*, 1995; *Beroza and Ellsworth*, 1996; *Lewis and Ben-Zion*, 2007]. More recently, new observations indicate that slow slip precedes and triggers the unstable ruptures phase [*Bouchon et al.*, 2011; *Kato et al.*, 2012; *Bouchon et al.*, 2013].

[3] Here we propose an experimental study of nucleation on a precut fault using polycarbonate as a rock-analog material. The dynamics of spontaneous rupture nucleation were monitored by both high-speed photoelasticity [*Nielsen et al.*, 2010] and high-frequency acoustic monitoring [*Schubnel et al.*, 2011]. After characterizing and describing the results of 47 experiments, we propose an empirical model, in which two parameters (critical nucleation length and surfacic power) control the scaling of the nucleation process. Finally, we discuss the relevance of these results by extrapolating them to the scale of natural faults.

2. Observation of Nucleation Phase

[4] We show three examples of characteristic videograms lasting 30 ms (Figure 1). The contrast of light intensity in the videograms allows us to track the position of the rupture tip in time (see "Methods" in supporting information and *Nielsen et al.* [2010] and *Schubnel et al.* [2011]). By inspection of Figure 1, it appears that the nucleation phase dynamics is controlled by the initial normal stress state: acceleration becomes more abrupt as normal stress increases. All the observed ruptures propagated in the same direction, which may be attributed to an inhomogeneous stress distribution on the fault produced by the load. Ruptures nucleate naturally, so that the position of the nucleation is not controlled and can vary. However, we observe that probably due to the initial stress distribution, the nucleation position does not vary of more than a centimeter between successive events. To characterize the nucleation phase dynamics, we construct a log-log diagram of the rupture velocity V_r as a function of the rupture length L (see Figure 2a and Methods) for 47 stick-slip events. The curves show an evolution of the rupture propagation divided in three distinct dynamic stages, each one characterized by a different slope of the $\log(V_r)$ versus $\log(L)$ curve. Following *Ohnaka and Shen* [1999], we name these stages, respectively, quasi-static stage (first low slope), acceleration stage (high slope), and dynamic propagation stage (final low slope). Depending on the event, it may occur that only the first two phases or the two final phases are identifiable in the images. In Figure 2a, the curves are visibly organized depending on the initial normal stress σ_0 of each event, indicating that average length and velocity in the initial phases decrease with increasing normal stress.

3. Empirical Model for Nucleation Dynamics

[5] We first characterize the rupture dynamics during the nucleation phase, then discuss the dependency on the normal initial stress. The first quasi-static phase is characterized by a log-log slope equal to 1, indicating linear dependence

Additional supporting information may be found in the online version of this article.

[1]Laboratory of Geology, UMR 8538, ENS and CNRS, Paris, France.
[2]Seismology and Tectonophysics Department, INGV, Roma, Italy.
[3]Earth Sciences Department, Durham University, Durham, U.K.
[4]Department of Geology, University of Leicester, Leicester, U.K.
[5]British Geological Survey, Environmental Science Centre, Nottingham, U.K.

Corresponding author: S. Latour, Laboratory of Geology, UMR 8538, ENS and CNRS, 24 Rue Lhomond, 75231 Paris CEDEX 5, France. (soumaya.latour@ens.fr)

0094-8276/13/10.1002/grl.50974

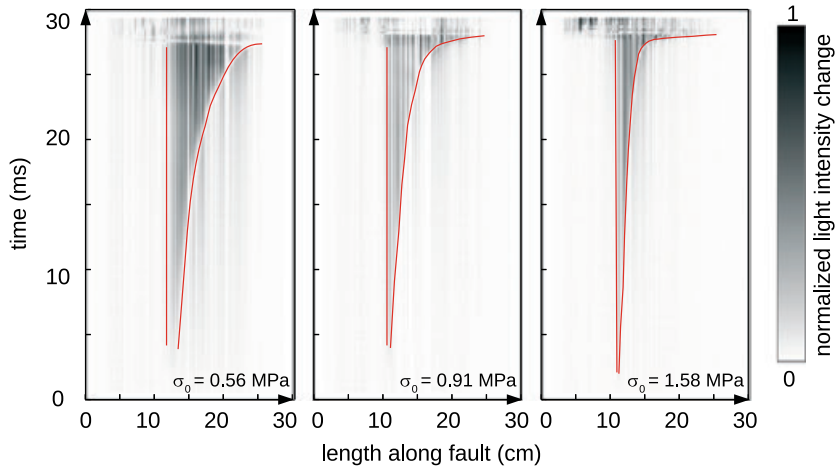

Figure 1. Three spontaneously nucleated laboratory earthquakes at increasingly higher normal prestresses. The gray scale corresponds to the light intensity change since time $t = 0$. The red curves highlight the position of rupture tips as a function of time.

between V_r and L. Therefore, during this phase, the rupture length grows exponentially as a function of time and is described by

$$L = L_0 e^{\frac{t-t_0}{t_c}} \qquad t < t_0 \tag{1}$$

where L_0 is the length of the rupture at the end of the quasi-static phase and t_0 is defined as the instant of the transition between the quasi-static and the acceleration phase. t_c is a characteristic time defined by $t_c = L_0/V_{r0}$ where V_{r0} is the velocity at time $t = t_0$. Time $t_0 = 0$ is arbitrarily defined as the last instant of exponential growth (quasi-static phase) and the beginning of the second phase (acceleration phase). The latter is characterized by slopes $n > 1$, indicating a differential equation of the type $V_r = CL^n$, where C is a proportionality constant. The continuity between the quasi-static phase and the acceleration phase at $t = t_0$ gives $C = t_c^{-1} L_0^{(1-n)}$. The solution of this differential equation is an inverse power law of time in the form

$$L = \frac{L_0}{\left(1 - \frac{(n-1)(t-t_0)}{t_c}\right)^{\frac{1}{(n-1)}}} \qquad t > 0 \tag{2}$$

[6] According to equation (2), L diverges at the instant $t_0 + t_f$, with $t_f = t_c/(n-1)$. The acceleration phase therefore stops short of diverging and the third stage of propagation starts. Here a much lower slope (between 0 and 1) in Figure 2a indicates high rupture velocities close to the shear wave speed c_s characterizing the dynamic rupture propagation. We note L_1 and V_{r1} the rupture length and rupture velocity at which the dynamic propagation stage begins. In the following, we will describe this last dynamic phase by a constant rupture velocity.

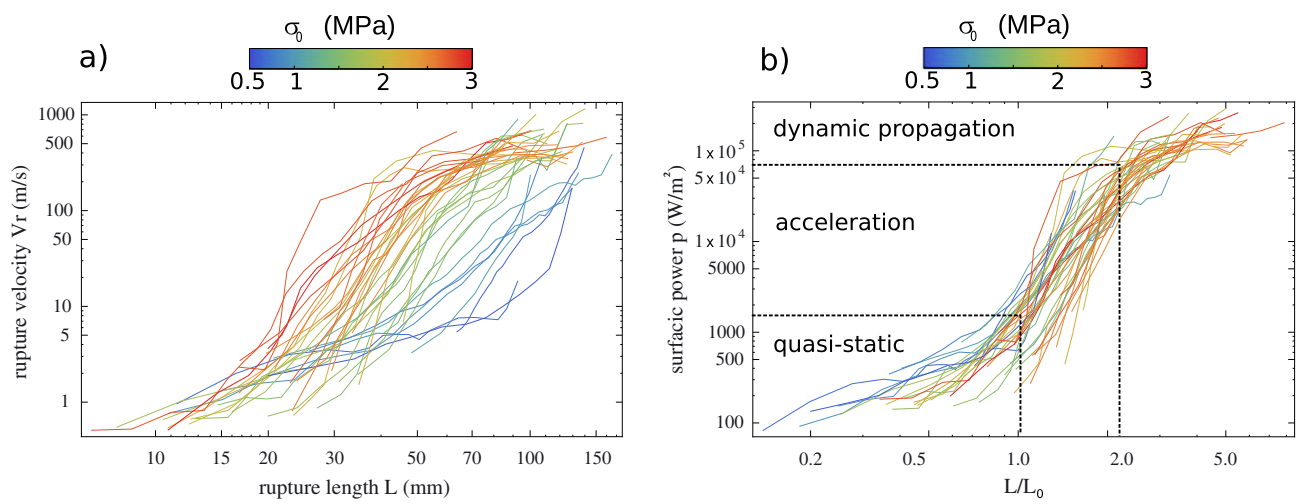

Figure 2. (a) Rupture velocity as a function of rupture length obtained from high-speed videos for 45 slip events (each curve represents a single rupture event). Changes in slope allow to distinguish different stages of dynamic rupture. The organization of the curves indicates a dependence with the initial normal stress (represented by color code). (b) The curves are collapsed by renormalizing the horizontal axis with $L_c \sim \sigma_0^{-1}$ and plotting the available surfacic power $p = k\tau_0 V_r$ instead of V_r in the vertical axes (see text for details). The three phases (quasi-static, acceleration, and dynamic propagation) of the dynamic evolution can be distinguished.

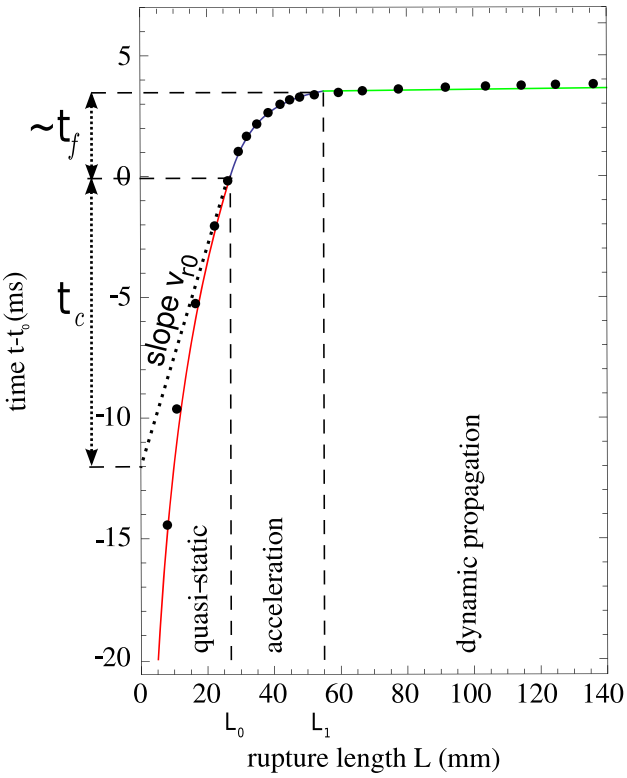

Figure 3. Experimental evolution of the rupture length as a function of time for one event (dots) and the fit with the empirical model in three phases (continuous colored lines). The quasi-static phase is described by equation (1), the acceleration phase is described by (2), and the dynamic propagation is described by a constant rupture velocity. For this particular event, we find $n = 4$, $t_c = 12$ ms, and $L_0 = 27$ mm.

[7] When comparing the data of a single slip event to this empirical model (see an example for one slip event in Figure 3), we find that the empirical model describes well the dynamics of the rupture nucleation and propagation once t_c, n, and L_0 are properly adjusted.

4. Scaling of the Nucleation Phase With Initial Stress

[8] We measure the length L_0 of the nucleation zone at the transition from the quasi-static to the acceleration phase) for all the events for which it is possible. Figure 4a shows that L_0 decreases as the inverse of σ_0. The best fit gives $L_0 = A/\sigma_0$ where $A = (56.3 \pm 14) \times 10^3$ Pa m. We use this relation to obtain a normalizing value for the rupture length L of each event, in order to obtain a dimensionless rupture length L/L_0. This scaling with σ_0 was proposed by several theoretical work [e.g., *Andrews*, 1976; *Okubo and Dieterich*, 1984; *Campillo and Ionescu*, 1997; *Rubin and Ampuero*, 2005]. For slip weakening friction, the critical nucleation length L_c is related to the friction parameters as follows [*Campillo and Ionescu*, 1997; *Favreau et al.*, 1999]:

$$L_c = \beta \frac{\mu D_c}{\sigma_0 (f_s - f_d)} \tag{3}$$

where f_s and f_d are the static and dynamic friction coefficients, D_c is the critical weakening distance, μ is the shear modulus, and the β is a nondimensional coefficient of the order $\beta = 1.158$ [*Campillo and Ionescu*, 1997; *Uenishi and Rice*, 2003]. Assuming that L_c corresponds to the measured length L_0 implies that D_c does not vary with the normal stress. This is probable in the explored range of normal stress (from 0 to 3 MPa). Assuming a complete stress drop (i.e., $f_s - f_d = 1$), $\mu = 957$ MPa ($c_s = 893$ m s^{-1}, $\rho = 1200$ kg m^{-3}), we obtain a maximal value for $D_c = 51$ µm. In the case of partial stress drop, D_c would be smaller. This value is in good agreement with a smooth surface in the laboratory, which tends to support the fact that $L_0 = L_c$. Note that in Figure 2b, the dynamic parts of the curves also collapse which may indicate that the inverse scaling with σ_0 also applies to the transition length to dynamic propagation L_1.

[9] We also observe that V_{r0} increases with decreasing initial stress (Figure 2a). Using the accelerometric measurements, we can relate the local rupture velocity to the local maximum slip velocity at the rupture tip (peak of particle velocity corresponding to the passage of the rupture front) over a wide range of rupture velocities V_r and associated

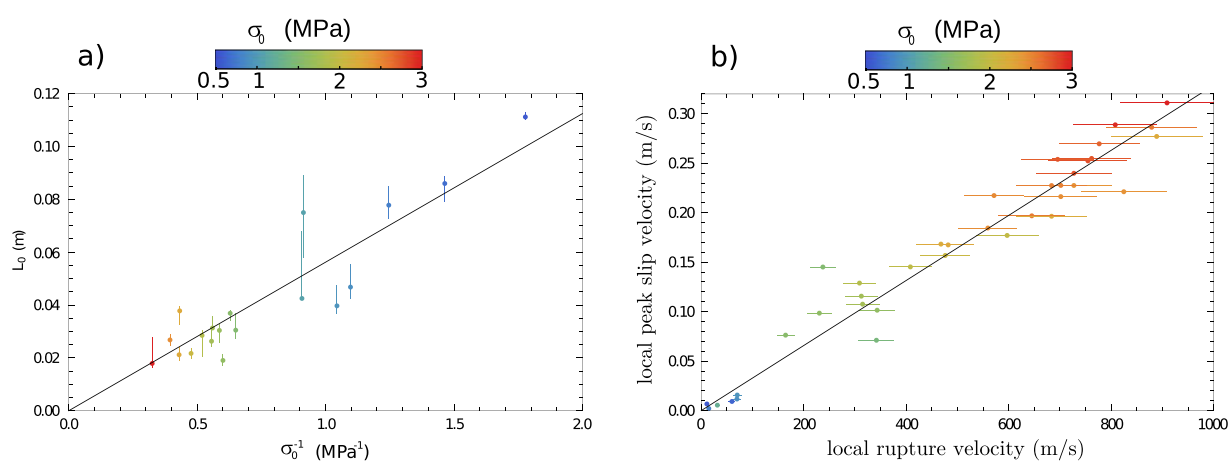

Figure 4. (a) Measured critical length L_0, corresponding to the transition from quasi-static to acceleration phase, as a function of the inverse of initial normal stress. (b) Near-field peak particle velocity (proportional to peak slip velocity) as a function of rupture velocity. The best linear fit are plotted in black in both figures. Color scale indicates the level of normal stress at the beginning of each event.

peak particle velocities $\dot{u}_{\max}$ (Figure 4b). $\dot{u}_{\max}$ varies linearly with V_r following $\dot{u}_{\max} = kV_r$, where k is a nondimensional proportionality factor that the best fit estimates to $k = 3.3 \times 10^{-4}$. The shear wave velocity being $c_s = 893\,\mathrm{m\,s^{-1}}$, the proportionality between the peak slip velocity and the rupture velocity is verified with no break for rupture velocities ranging from $0.01c_s$ to c_s, in the limit of the available precision. This linear relationship allows to estimate the peak slip velocity at the rupture tip, so that in each experiment, the critical rupture velocity v_{r0} is uniquely related to a critical slip velocity.

[10] The variation of the critical velocity V_{r0} with initial stress σ_0 may then be understood when estimating the surfacic power p available at the rupture tip at each instant by using [*Di Toro et al.*, 2011]

$$p = \tau_0 \dot{u}_{\max} = k\tau_0 V_r \tag{4}$$

[11] In Figure 2b, we plot p as a function of the dimensionless rupture length L/L_0 in log scale. Because p is proportional to V_r, each curve is rescaled, preserving the same shape as in Figure 2a and the quasi-static, acceleration, and dynamic propagation phases can be clearly distinguished. Figure 2b shows that all the individual curves collapse in a consistent way, indicating that p and L/L_0 are the appropriate scaling parameters. For all the events, the passage from the quasi-static to the acceleration phase is defined by a critical surfacic power $p_0 = 1600 \pm 600\,\mathrm{W\,m^{-2}}$ so that p_0 may be interpreted as a unique characteristic value of the interface. More specifically, the parameter L_0 controls the length at which instability begins while the power parameter p_0 controls the rupture acceleration with respect to the frictional power dissipated on the fault. In fact, both L/L_0 and p result from multiplying by the stress either the length or the velocity, respectively (excluding additional normalizing terms). As a consequence, with increasing normal stress, the nucleation curve preserves the same shape, but it is contracted in both length and velocity in proportion to σ_0. The transition from the acceleration to the dynamic propagation phases also occurs at a critical power that we can note p_1, with $p_1 \simeq 10^5\,\mathrm{W\,m^{-2}}$.

5. Discussion

[12] *Ohnaka and Shen* [1999] also observed a very slow phase before the acceleration phase in the nucleation of ruptures between two blocks of Westerly granite [see also *Ohnaka and Shen*, 1999 and *Ohnaka*, 2003], and *Nielsen et al.* [2010] reported similar behavior in stick-slip experiments on analog synthetic material. However, they describe this phase as an expansion at constant velocity of a stable rupture. In our case, the first phase does not grow at constant velocity. On the contrary, the rupture velocity grows exponentially during this stage. This is especially clear for the events occurring at low initial stress, because the quasi-static phase in these events lasts until the rupture reaches relatively large length and velocity. This exponential growth is interesting because it strongly suggests that during this phase, the fault is already unstable, which would not be the case if the rupture grew at constant velocity.

[13] The exponential growth which we observe thanks to the resolution of our high-speed photographic observations could well have been present also in the previous studies reporting an apparent constant velocity. Indeed, due to the relatively slow takeoff and with low resolution of the data, it may have been impossible to distinguish it from a linear trend. However, two other hypotheses cannot be discarded: It is possible that the dynamics of this phase depends on the materials in contact, or it may be that it is extremely dependent to the loading process, which in our case is not well controlled.

[14] The passage from one phase to the following is controlled by a critical power available at the rupture tip. Depending on the available power, different physical processes may occur at the rupture tip. We propose that during the first quasi-static phase, the slow propagation is due to quasi-static stress transfer at the rupture tip and subsequent slow failure. However, this process being unstable, the slip velocity slowly grows. p_0 may be the critical power at which pronounced weakening is triggered at the rupture tip and acceleration of rupture ensues. The concept of critical power is close to that of effective fracture energy, but it contains the idea that to dynamically break the interface, the fracture energy must be supplied at a high enough rate. This may be due to a balance between the rate of the physical phenomena that tend to concentrate the energy at the interface (mainly stress concentration) and transport phenomenon that can evacuate it (thermal or physical diffusion, viscosity, etc.). For example *Di Toro et al.* [2011] showed that in the case of rocks, pronounced weakening is associated to a critical frictional power in experimental tests. The weakening is associated with thermally activated physical (melting) or chemical (dehydration, decarbonation) phenomenon. In a similar manner, *Rice* [2006] discussed early frictional weakening as plastic failure of asperities (flash weakening) due to sliding. The physical reasons of the weakening in our case are still to be elucidated and are certainly quite different from those occurring in faults.

[15] Weakening increases the rupture velocity and consequently, the slip velocity and the available power at the tip. In such way, the weakening is self-sustained and enhanced, which induces the acceleration of the rupture tip. The acceleration phase can be explained, qualitatively, using a modified Charles law for mode II cracks, where the rupture velocity and stress intensity factor are related by a power law of the form: $V_r = k_2\, K_{II}^{2n}$. Indeed, remembering that the static stress intensity factor $K_{II} = \tau_0 \sqrt{\frac{\pi L}{2}}$, we obtain the observed relation $v_R \alpha L^n$. In mode I, Charles's law is characteristic of subcritical crack growth and brittle creep [*Brantut et al.*, 2013].

[16] Rupture accelerates until the second critical power p_1 is reached. We assume that this power corresponds to a maximum rate at which the weakening mechanism can consume energy. Subsequently, weakening becomes constant and the rupture acceleration decreases to values close to 0, corresponding to rupture propagation at near constant velocity. This is the dynamic propagation phase. During this phase, the excess of power available at the rupture tip is radiated away by elastic waves. We should note that although we did not observe such cases, if the rupture was to reach the P wave velocity before reaching p_1, then it would stop at this physical limit and deviate from the general scaling.

6. Conclusion

[17] The characteristic time of the nucleation phase, t_c, quantify both the exponential growth of the quasi-static

evolution (equation (1)) and the duration of the acceleration phase (equation (2)). It does not depend on the initial stress and is defined by $t_c = L_0/v_{r0}$. The quasi-static phase is very long and has no definite beginning, hence no definite duration. The time during which rupture accelerates, in contrast, is well defined and relatively short (see Figure 3). More precisely, the duration of the acceleration phase is characterized by the exponent n and t_c and is approximately $t_f = t_c/(n-1)$. In our case, $n = 5 \pm 1$ for all events, with no clear variation with stress. The order of magnitude of t_f is the same for all the events. Using equations (3) and (4), we obtain

$$t_c = \frac{k\mu}{p_0}\frac{D_c}{f_s - f_d} \tag{5}$$

[18] Following this equation, t_c is determined by the elastic properties of the material and the properties of the interface. With the measured values in our experiments, we obtain values for t_c ranging between 5 and 15ms. To extrapolate to natural conditions, we must remember that D_c is scale dependent [*Ohnaka*, 2003]. For large earthquakes, D_c may be of the order 1 m. $(f_s - f_d)$ is not known and will be taken equal to 1. It is reasonable to suppose that the larger the stress drop, the larger the value of $(f_s - f_d)$, hence the shortest the characteristic time t_c. Actually, what appears in the characteristic time is the inverse of the slip weakening rate $(f_s - f_d)/D_c$, a parameter that has been demonstrated to be scale dependent due to the heterogeneity of faults at all scales, and to grow with the scale of observation [*Latour et al.*, 2011]. From *Di Toro et al.* [2011], p_0 for rocks can be estimated between 10^4 and 10^5 W m^{-2}. However, we do not have any information on how this value scales with the observation scale. The proportionality factor k between v_r and $\dot{u}_{\max}$ can be estimated by using usual slip velocities (1 m s^{-1}) and rupture velocities ($v_r \simeq 3000$ m s^{-1}) for earthquakes. This gives $k = 0.33 \times 10^{-3}$, i.e., the same value that we measured in our experiments. With these values, the expression (5) gives $t_c \simeq 90$ to 900 s, i.e., acceleration phases lasting for $t_f \simeq 22$ to 225 s, from few seconds to few minutes. If the hypotheses made before are correct, this would be the order of magnitude of the acceleration phase duration. However, the value of p_0, a still new and not widely discussed concept, is largely uncertain.

[19] Another kind of estimation can be made in relation to seismic observation of the quasi-static phase. Indeed, if the slow rupture velocity and the ruptured length can be estimated during this phase, the characteristic time is given by $t_c = L/v_r$. A slow migration of low seismicity preceding the Mw 9.0 2011 Tohoku-Oki earthquake has been interpreted as a nucleation process by *Kato et al.* [2012]. The active fault length in which seismicity occurs is about 50 km long while its growth velocity is about 5 km/day. Using these values and supposing that the slow slip corresponds to the quasi-static phase, we obtain a characteristic time $t_c = 10$ days. It is striking that the Mw 7.3 foreshock occurred 10 days after the end of this seismic activity and the main shock 12 days after. These durations are thus compatible with the order of magnitude of t_c. However, this estimation does not agree with the previously estimated t_c that used p_0. While our very simple analog experimental model most probably cannot apply directly to earthquakes that are much more complex (rough heterogeneous 2-D fault, larger scale, different material, etc.), it nevertheless provides a model for nucleation process in the frame of which seismic observations can be discussed.

[20] To conclude, our main results are (1) the existence of two phases in the nucleation process, (2) their characterization, and (3) their inverse scaling with the initial stress. These observations may lead to a better understanding of the development of slip instability and of the earthquake source.

[21] **Acknowledgments.** We thank Jacopo Taddeucci and Yves Pinquier for their technical support. This project was funded through CNRS-INSU (project SILENS) and the French Ministry of Foreign Affairs (program Galileo). Partial support has been provided through grant ANR-2011-BS56-017 of the French "Agence Nationale de la Recherche."

[22] The Editor thanks Gregory McLaskey and an anonymous reviewer for their assistance in evaluating this paper.

References

Ampuero, J.-P., and A. M. Rubin (2008), Earthquake nucleation on rate and state faults–Aging and slip laws, *J. Geophys. Res.*, *113*, B01302, doi:10.1029/2007JB005082.

Andrews, D. J. (1976), Rupture velocity of plane strain shear cracks, *J. Geophys. Res.*, *81*(32), 5679–5687.

Beroza, G. C., and W. L. Ellsworth (1996), Properties of the seismic nucleation phase, *Tectonophysics*, *261*, 209–227.

Bouchon, M., H. Karabulut, M. Aktar, S Özalaybey, J. Schmittbuhl, and M.-P. Bouin (2011), Extended nucleation of the 1999 Mw 7.6 Izmit earthquake, *Science*, *331*, 877–880.

Bouchon, M., V. Durand, D. Marsan, H Karabulut, and J. Schmittbuhl (2013), The long precursory phase of most large interplate earthquakes, *Nat. Geosci.*, *6*, 299–302.

Brantut, N., M. J. Heap, P. G. Meredith, and P. Baud (2013), Time-dependent cracking and brittle creep in crustal rocks: A review, *J. Struct. Geol.*, *52*(0), 17–43.

Campillo, M., and I. R. Ionescu (1997), Initiation of antiplane shear instability under slip dependent friction, *J. Geophys. Res.*, *102*(B9), 20,363–20,371.

Di Toro, G, R. Han, T. Hirose, N. De Paola, K. Nielsen, S. Mizoguchi, F. Ferri, M. Cocco, and T. Shimamoto (2011), Fault lubrication during earthquakes, *Nature*, *471*, 494–498.

Dieterich, J. H. (1978), Preseismic fault slip and earthquake prediction, *J. Geophys. Res.*, *83*(B8), 3940–3948.

Favreau, P., M. Campillo, and I. R. Ionescu (1999), Initiation of in-plane shear instability under slip-dependent friction, *Bull. Seismol. Soc. Am.*, *89*(5), 1280–1295.

Ida, Y. (1972), Cohesive force across the tip of a longitudinal-shear crack and Griffith's specific surface energy, *J. Geophys. Res.*, *77*(20), 3796–3805.

Iio, Y. (1995), Observations of the slow initial phase generated by microearthquakes: Implications for earthquake nucleation and propagation, *J. Geophys. Res.*, *100*(B8), 15,333–15,349.

Kaneko, Y., and J.-P. Ampuero (2011), A mechanism for preseismic steady rupture fronts observed in laboratory experiments, *Geophys. Res. Lett.*, *38*, L21307, doi:10.1029/2011GL049953.

Kato, A., K. Obara, T. Igarashi, H. Tsuruoka, S. Nakagawa, and N. Hirata (2012), Propagation of slow slip leading up to the 2011 Mw 9.0 Tohoku-Oki earthquake, *Science*, *335*(6069), 705–708.

Latour, S., M. Campillo, C. Voisin, I. R. Ionescu, J. Schmedes, and D. Lavalle (2011), Effective friction law for small-scale fault heterogeneity in 3D dynamic rupture, *J. Geophys. Res.*, *116*, B10306, doi:10.1029/2010JB008118.

Lewis, M. A., and Y. Ben-Zion (2007), Examination of scaling between proposed early signals in *P* waveforms and earthquake magnitudes, *Geophys. J. Int.*, *171*, 1258–1268.

McLaskey, G. C., and B. D. Kilgore (2013), Foreshocks during the nucleation of stick-slip instability, *J. Geophys. Res. Solid Earth*, *118*, 2982–2997, doi:10.1002/jgrb.50232.

Nielsen, S., J. Taddeucci, and S. Vinciguerra (2010), Experimental observation of stick-slip instability fronts, *Geophys. J. Int.*, *180*(2), 697–702.

Ohnaka, M. (2003), A constitutive scaling law and a unified comprehension for frictional slip failure, shear fracture of intact rock, and earthquake rupture, *J. Geophys. Res.*, *108*(B1), 2080, doi:10.1029/2000JB000123.

Ohnaka, M., and L. F. Shen (1999), Scaling of the shear rupture process from nucleation to dynamic propagation: Implications of geometric irregularity of the rupturing surfaces, *J. Geophys. Res.*, *104*(B1), 817–884.

Okubo, P. G., and J. H. Dieterich (1984), Effects of physical fault properties on frictional instabilities produced on simulated faults, *J. Geophys. Res.*, *89*(B7), 5817–5827.

Rice, J. R. (2006), Heating and weakening of faults during earthquake slip, *J. Geophys. Res.*, *111*, B05311, doi:10.1029/2005JB004006.

Rubin, A. M., and J.-P. Ampuero (2005), Earthquake nucleation on (aging) rate and state faults, *J. Geophys. Res.*, *110*, B11312, doi:10.1029/2005JB003686.

Schubnel, A., S. Nielsen, J. Taddeucci, S. Vinciguerra, and S. Rao (2011), Photo-acoustic study of subshear and supershear ruptures in the laboratory, *Earth Planet. Sci. Lett.*, *308*, 424–432.

Uenishi, K., and J. R. Rice (2003), Universal nucleation length for slip-weakening rupture instability under nonuniform fault loading, *J. Geophys. Res.*, *108*(B1), 2042, doi:10.1029/2001JB001681.